PERGAMON

International Journal of Heat and Mass Transfer 42 (1999) 2465–2481

International Journal of HEAT and MASS TRANSFER

Mixed convection flow in a lid-driven enclosure filled with a fluid-saturated porous medium

Khalil M. Khanafer, Ali J. Chamkha*

Kuwait University, College of Engineering and Petroleum, Department of Mechanical and Industrial Engineering, P.O. Box 5969, Safat, Kuwait 13060

Received 12 February 1998; in final form 10 July 1998

Abstract

Volume averaged equations governing unsteady, laminar, mixed convection flow in an enclosure filled with a Darcian fluid-saturated uniform porous medium in the presence of internal heat generation is formulated. The two vertical walls of the enclosure are insulated while the horizontal walls are kept at constant temperatures with the top surface is moving at a constant speed. The developed equations are nondimensionalized and then solved numerically subject to appropriate initial and boundary conditions by the finite-volume approach along with the alternating direct implicit (ADI) procedure. Comparisons with previously published work are performed and found to be in excellent agreement. A parametric study is conducted and a set of graphical results is presented and discussed to elucidate interesting features of the solution.

Key words: Mixed convection; Heat generation; Porous medium

Nomenclature

$a_{i,j}$ coefficient of finite difference equation at point (i, j) in a grid
b right-hand side of finite difference equation
c_p fluid specific heat [J kg^{-1} K^{-1}]
Da Darcy number, κ/H^2
Da^{-1} inverse Darcy number $(1/Da)$
g gravitational acceleration [m s^{-2}]
Gr Grashof number, $g\beta\Delta TH^3/\nu^2$
H enclosure length [m]
K_e effective thermal conductivity of the porous medium [W m^{-1} K^{-1}]
M grids number in x-direction
N grids number in y-direction
$\overline{Nu}$ average Nusselt number, $\overline{Nu}=\int_0^1[(\partial\theta/\partial Y)-Pr\ Re\ V]\,dX$
P fluid pressure [Pa]
Pr Prandtl number, ν/α_e
q''' volumetric heat generation
Re Reynolds number, U_0H/ν_e
Ra_E external Rayleigh number, $g\beta\Delta TH^3/\nu\alpha_e$
Ra_I internal Rayleigh number, $g\beta q'''H^5/\nu\alpha_eK_e$
t time [s]
T temperature [°C]
u velocity in x-direction
U dimensionless x-component of velocity, u/U_0
U_c dimensionless velocity in x-direction at mid-height of enclosure
U_0 lid velocity
v velocity in y-direction
V dimensionless y-component of velocity, v/U_0
V_c dimensionless velocity in y-direction at mid-width of enclosure
x, y Cartesian coordinates
X, Y dimensionless Cartesian coordinates, $(x, y)/H$.

Greek symbols

α_e effective thermal diffusivity of porous medium [m^2 s^{-1}]
β coefficient of thermal expansion of fluid [K^{-1}]
ΔT temperature difference
θ dimensionless temperature, $(T-T_C)/(T_H-T_C)$
κ permeability of the porous medium [m^2]

* Corresponding author.

0017-9310/99/$ - see front matter
PII: S0017-9310(98)00227-0

μ effective dynamic viscosity [Pa s^{-1}]
ν effective kinematic viscosity, μ/ρ_0
ρ_0 fluid density at reference temperature T_C
τ dimensionless time, tU_0/H
ψ stream function [m^2 s^{-1}]
ψ dimensionless stream function, ψ/HU_0
ω dimensionless vorticity, $\Omega H/U_0$
Ω dimensional vorticity, $(\partial v/\partial x)-(\partial u/\partial y)$.

Subscripts
C cold wall
H hot wall
i X location of a grid point
j Y location of a grid point.

1. Introduction

Mixed convection flow and heat transfer in enclosures is of interest in engineering and science. Its applications include nuclear reactors [1], lakes and reservoirs [2], solar collectors [3], and crystal growth. Moreover, the flow and heat transfer in a shear driven cavity arises in industrial processes such as food processing and float glass production [4].

The problem of a lid-driven cavity flow in enclosures has been used extensively as a standard test case for the evaluation of numerical solution procedures for the Navier–Stokes equations [5–10]. Koseff and Street [11] have studied experimentally as well as numerically the recirculation flow patterns for a wide range of Reynolds and Grashof numbers. Their results show that the three-dimensional features, such as corner eddies near the end walls, and Taylor–Gortler-like longitudinal vortices, have significant effects on the flow patterns for low Reynolds numbers. Both thermally stable and unstable lid-driven flows inside enclosures have been investigated numerically by Torrance et al. [12] for fixed values of Reynolds and Prandtl numbers. Their numerical results have indicated that the Richardson number is a controlling parameter for the problem. Recently, Prasad and Koseff [13] have performed an experimental investigation of a recirculating mixed convection flow in a cavity filled with water. For the range of the governing parameters studied, their results indicate that the overall heat transfer rate is a very weak function of the Grashof number for the examined range of the Reynolds number. The effects of the Prandtl number on laminar mixed convection heat transfer in a lid-driven cavity have been considered numerically by Moallemi and Jang [14]. Their numerical simulations have revealed that the influence of the buoyancy on the flow and heat transfer inside cavities is predicted to be more pronounced for higher values of the Prandtl number. Later on, Iwatsu et al. [15] have studied numerically mixed convection heat transfer in a driven cavity with a stable vertical temperature gradient. Their results have shown that the flow features are similar to those of a conventional driven-cavity of a non-stratified fluid for small values of the Richardson number. Also, it has been found that when the Richardson number is very high, much of the middle and bottom portions of the cavity interior is stagnant.

Flow through a confined porous medium has drawn considerable attention in the last few years due to the large number of technological and industrial applications such as geothermal energy systems, prevention of sub-oil water pollution, storage of nuclear waste, etc. (see, for instance, Kakak et al. [16] and Bejan [17]). Free convection heat transfer in a porous medium has been studied extensively in the literature. Cheng [18] provides an extensive review of the literature on free convection in fluid-saturated porous media with regard to applications in geothermal systems. The state of art regarding porous media models has been summarized in a recent book by Nield and Bejan [19].

Early works on flow in porous media have used the Darcy law which is applicable to slow flows and does not account for inertial and boundary effects (termed as non-Darcy effects) which become important when the flow velocity is relatively high and in the presence of a boundary. The condition of high velocity is realized when the pressure across the porous medium is a quadratic function of the velocity. Vafai and Tien [20] have reported a detailed discussion on these non-Darcian effects. Mixed convection flows along vertical plates and other geometries embedded in porous media with Darcian and non-Darcian effects have been reported by many authors (e.g. [21–25]).

The objective of the present work is to consider the Brinkman-extended Darcy equation of motion with the convective terms included and to examine the influence of the Richardson number, Darcy number, and the internal Rayleigh number on mixed convection flow inside a square enclosure filled with a fluid-saturated porous medium. Therefore, a two dimensional numerical model will be used to solve the vorticity, stream function and energy equations governing buoyancy-driven mixed convection flow inside a cavity.

2. Problem formulation

The physical model considered in this investigation is shown in Fig. 1. A two-dimensional square enclosure of height H is filled with a fluid-saturated porous medium of uniform porosity and permeability which generates heat at a uniform rate. The top surface of the enclosure is moving from left to right at a constant speed U_0. The two vertical walls of the enclosure are insulated while the top lid and the bottom surfaces are maintained at constant temperatures, T_H and T_C, respectively such that $T_H > T_C$. The directions of the acceleration due to gravity

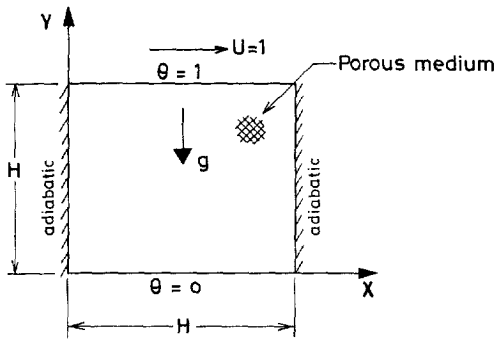

Fig. 1. Flow configuration and coordinate system.

g and the coordinate axes are also shown in Fig. 1. The porous medium is assumed to be hydrodynamically and thermally isotropic and saturated with a fluid that is in local thermodynamic equilibrium with the solid matrix. The flow in the above problem is assumed to be unsteady, laminar, incompressible, and the fluid physical properties are assumed constant except the density variation in the body force term of the momentum equation according to the Boussinesq approximation. In addition, pressure work, and viscous dissipation are all assumed negligible.

The governing equations of the problem under consideration are based on the balance laws of mass, linear momentum, and thermal energy. Taking into account the above mentioned assumptions, these equations, expressed in dimensional form, can be written as

$$\frac{\partial u}{\partial x}+\frac{\partial v}{\partial y}=0 \tag{1}$$

$$\frac{\partial u}{\partial t}+u\frac{\partial u}{\partial x}+v\frac{\partial u}{\partial y}=-\frac{1}{\rho_0}\frac{\partial P}{\partial x}+\nu\left(\frac{\partial^2 u}{\partial x^2}+\frac{\partial^2 u}{\partial y^2}\right)-\frac{\mu u}{\rho_0 \kappa} \tag{2}$$

$$\frac{\partial v}{\partial t}+u\frac{\partial v}{\partial x}+v\frac{\partial v}{\partial y}=-\frac{1}{\rho_0}\frac{\partial P}{\partial y}+\nu\left(\frac{\partial^2 v}{\partial x^2}+\frac{\partial^2 v}{\partial y^2}\right)+g\beta(T-T_C)-\frac{\mu v}{\rho_0 \kappa} \tag{3}$$

$$\frac{\partial T}{\partial t}+u\frac{\partial T}{\partial x}+v\frac{\partial T}{\partial y}=\frac{K_e}{\rho_0 c_p}\left(\frac{\partial^2 T}{\partial x^2}+\frac{\partial^2 T}{\partial y^2}\right)+\frac{q'''}{\rho_0 c_p} \tag{4}$$

where u and v are the pore velocity components in the x- and y-directions, respectively. t is the time, T is the fluid temperature, P is the fluid pressure, β is the volumetric thermal expansion coefficient, κ is the permeability of the porous medium, and K_e, ν, μ, ρ_0, and c_p are the effective thermal conductivity of the porous medium, effective kinematic viscosity, effective dynamic viscosity, fluid density, and the specific heat, respectively. q''' is the volumetric internal heat generation. It should be noted that Eqs. (2) and (3) do not include the porous medium inertia effects which have been shown by many investigators such as Lage [26] and Chan et al. [27] to have very little effect on heat transfer. This will be in line with the problem considered herein when the Reynolds number is small.

The initial and boundary conditions for the above system of equations corresponding to the geometry in Fig. 1 can be written as follows:

$$\left.\begin{aligned} &u=v=0, && T=0 && \text{at all } x, y \text{ and } t<0\\ &u=v=0 && \text{on } x=0,H; && y=0,H\\ &\frac{\partial T}{\partial x}=0 && \text{on } x=0,H\\ &T=T_H && \text{on } y=H\\ &T=T_C && \text{on } y=0 && \text{for } t\geqslant 0. \end{aligned}\right\} \tag{5}$$

It is convenient to non-dimensionalize Eqs. (1)–(5) using the following dimensionless variables:

$$\left.\begin{aligned} &X=\frac{x}{H}, && Y=\frac{y}{H}\\ &U=\frac{u}{U_0}, && V=\frac{v}{U_0}\\ &\theta=\frac{T-T_C}{T_H-T_C}, && \tau=\frac{tU_0}{H}\\ &\omega=\frac{\Omega H}{U_0}, && \Psi=\frac{\psi}{HU_0} \end{aligned}\right\} \tag{6}$$

where ψ and Ω are the dimensional stream function and vorticity, respectively.

Defining the stream function ψ and the vorticity Ω (see the nomenclature section) in the usual way and substituting Eqs. (6) into the previous governing equations results in the following dimensionless equations:

$$\omega=-\left(\frac{\partial^2\Psi}{\partial X^2}+\frac{\partial^2\Psi}{\partial Y^2}\right) \tag{7}$$

$$U=\frac{\partial\Psi}{\partial Y},\quad V=-\frac{\partial\Psi}{\partial X} \tag{8}$$

$$\frac{\partial\omega}{\partial\tau}+U\frac{\partial\omega}{\partial X}+V\frac{\partial\omega}{\partial Y}=\frac{1}{Re}\left(\frac{\partial^2\omega}{\partial X^2}+\frac{\partial^2\omega}{\partial Y^2}\right)+\frac{Gr}{Re^2}\frac{\partial\theta}{\partial X}-\frac{\omega}{Da\,Re} \tag{9}$$

$$\frac{\partial\theta}{\partial\tau}+U\frac{\partial\theta}{\partial X}+V\frac{\partial\theta}{\partial Y}=\frac{1}{Pr\,Re}\left(\frac{\partial^2\theta}{\partial X^2}+\frac{\partial^2\theta}{\partial Y^2}\right)+\frac{Ra_I}{Ra_E}\frac{1}{Pr\,Re} \tag{10}$$

where

$$Re=\frac{U_0 H}{\nu},\quad Gr=\frac{g\beta\Delta T H^3}{\nu^2},$$

$$Da = \frac{\kappa}{H^2}, \quad Pr = \frac{\nu}{\alpha_e},$$

$$Ra_I = \frac{g\beta q''' H^5}{\nu\alpha_e K_e}, \quad \text{and} \quad Ra_E = \frac{g\beta\Delta T H^3}{\nu\alpha_e}$$

are the Reynolds number, Grashof number, Prandtl number, internal Rayleigh number, and the external Rayleigh number, respectively.

The dimensionless initial and boundary conditions of the problem under consideration can be written as

$$\begin{aligned} &U = V = \Psi = \theta = 0 \quad \text{for } \tau = 0 \\ &U = V = \Psi = 0 \quad \text{on all boundaries} \\ &\theta = 0 \quad \text{at } Y = 0 \\ &\theta = 1 \quad \text{at } Y = 1 \quad \text{for } \tau > 0. \end{aligned} \tag{11}$$

Eqs. (9) and (10) governing ω and θ can be cast in the general canonical form (see Patankar [28]) as:

$$\frac{\partial\phi}{\partial\tau} + \frac{\partial}{\partial X}\left[U\phi - \Gamma_\phi\frac{\partial\phi}{\partial X}\right] + \frac{\partial}{\partial Y}\left[V\phi - \Gamma_\phi\frac{\partial\phi}{\partial Y}\right] = S_\phi \tag{12}$$

where ϕ stands for ω or θ and Γ_ϕ and S_ϕ are given by

$$\begin{aligned} &\Gamma_\theta = \frac{1}{Pr\,Re}, \quad S_\theta = \frac{Ra_I}{Ra_E}\cdot\frac{1}{Pr\,Re} \\ &\Gamma_\omega = \frac{1}{Re}, \quad S_\omega = \frac{Gr}{Re^2}\frac{\partial\theta}{\partial X} - \frac{\omega}{Da\,Re}. \end{aligned} \tag{13}$$

The average Nusselt number at a given height of the enclosure may be expressed as

$$\overline{Nu} = \int_0^1 \left(\frac{\partial\theta}{\partial Y} - Pr\,Re\,V\right)dX. \tag{14}$$

In the above, the first and second terms denote the contributions from the conductive and the convective heat-transfer modes, respectively.

3. Numerical algorithm

In the present work, the control volume method [28] is used to solve the transient dimensionless governing Eqs. (7)–(10) subject to their corresponding initial and boundary conditions given in Eqs. (11). In this algorithm, the alternating direct implicit (ADI) procedure along with the successive grid refinement scheme are respectively implemented in the spatial and temporal environments to accelerate the convergence of the solution towards steady state. Additionally, the application of the ADI procedure enhances the accuracy of the solution since it allows the power-law scheme to be applied locally in a one-dimensional sense for each sweep in the coordinate directions. The finite-difference formulation of the general Eq. (12) in both X- and Y-directions, respectively are given by:

$$\left.\begin{aligned} &-a_{i-1,j}^{n+(1/2)}\phi_{i-1,j}^{n+(1/2)} + a_{i,j}^{n-(1/2)}\phi_{i,j}^{n+(1/2)} - a_{i+1,j}^{n+(1/2)}\phi_{i+1,j}^{n+(1/2)} = b^n \\ &-a_{i,j-1}^{n+1}\phi_{i,j-1}^{n+1} + a_{i,j}^{n+1}\phi_{i,j}^{n+1} - a_{i,j+1}^{n+1}\phi_{i,j+1}^{n+1} = b^{n-(1/2)} \end{aligned}\right\} \tag{15}$$

where the subscripts i and j denote the X and Y locations of the grid point, respectively. The superscripts n, $n+1/2$, and $n+1$ denote old time, advanced half-time step and advanced full-time step, respectively. The coefficients of Eqs. (15) are given by Patankar [28]. Therefore, for brevity, they will not be presented here.

To complete the discretization process, the flow kinematics Eq. (7) is discretized using central finite difference with successive over-relaxation (SOR) procedure. The final form of the equation becomes

$$\begin{aligned} \Psi_{i,j}^{n+1} = (\Psi_{i,j}^{n+1})^k + \frac{\lambda}{2(1+\varepsilon^2)} \\ \left[\begin{aligned} &(\Psi_{i+1,j}^{n+1})^k + (\Psi_{i-1,j}^{n+1})^{k+1} + \varepsilon^2\{(\Psi_{i,j-1}^{n+1})^k + (\Psi_{i,j-1}^{n+1})^{k+1}\} \\ &-2(1+\varepsilon^2)(\Psi_{i,j}^{n+1})^k + \Delta X^2\omega_{i,j}^{n+1} \end{aligned}\right] \end{aligned} \tag{16}$$

where ε is the ratio of the step sizes, such that $\varepsilon = \Delta X/\Delta Y$, n and k are the time step and the iteration step, respectively, and λ represents the relaxation factor which is given by

$$\begin{aligned} &\lambda = \frac{8-4\sqrt{4-\delta^2}}{\delta^2}, \\ &\delta = \cos\left(\frac{\pi}{M}\right) + \sin\left(\frac{\pi}{N}\right) \end{aligned} \tag{17}$$

where M and N are the total number of grid points along the X- and Y-directions, respectively. Once $\psi_{i,j}^{n+1}$ is calculated from Eq. (16), $U_{i,j}^{n+1}$, $V_{i,j}^{n+1}$ are then computed from

$$\left.\begin{aligned} U_{i,j}^{n+1} &= \frac{\Psi_{i,j+1}^{n+1} - \Psi_{i,j-1}^{n+1}}{2\Delta Y} \\ V_{i,j}^{n+1} &= \frac{\Psi_{i-1,j}^{n+1} - \Psi_{i+1,j}^{n+1}}{2\Delta X} \end{aligned}\right\} \tag{18}$$

In addition to the distributions of U and V, the vorticity on the boundaries can be computed according to the following expressions which are obtained from Eq. (7):

$$\left.\begin{aligned} \omega_{i,1} &= -\frac{(2\Psi_{i,1} - 5\Psi_{i,2} + 4\Psi_{i,3} - \Psi_{i,4})}{\Delta Y^2} \\ \omega_{i,N} &= -\frac{(2\Psi_{i,N} - 5\Psi_{i,N-1} + 4\Psi_{i,N-2} - \Psi_{i,N-3})}{\Delta Y^2} \\ \omega_{1,j} &= -\frac{(2\Psi_{1,j} - 5\Psi_{2,j} + 4\Psi_{3,j} - \Psi_{4,j})}{\Delta X^2} \\ \omega_{M,j} &= -\frac{(2\Psi_{M,j} - 5\Psi_{M-1,j} + 4\Psi_{M-2,j} - \Psi_{M-3,j})}{\Delta X^2}. \end{aligned}\right\} \tag{19}$$

4. Solution procedure

1. Use the temperatures of the previous time step as an initial guess. For the first time step, the initial temperature will be used to initiate the numerical computation.
2. Choose the trial values for U^n and V^n as the first approximations of U^{n+1} and V^{n+1}.
3. Compute the new values of the temperature at each grid point using Eq. (15) with ϕ playing the role of θ.
4. Use the values of the vorticities of the previous time step as initial guesses. For the first time step, the vorticities are assumed to be zero everywhere to initiate the solution.
5. Use the values of U^{n+1}, V^{n+1} and θ^{n+1} to compute the values of ω^{n+1} from Eq. (15) at the interior grid points.
6. Solve the stream function Eq. (16) using the new values of the vorticities obtained in step (5) above.
7. Determine the new values of U^{n+1} and V^{n+1} from the values of ψ^{n+1} using the central difference formulae given by Eqs. (18).
8. Compute the new boundary vorticities using the values of ψ^{n+1} according to Eqs. (19).
9. Use the new values of U^{n+1} and V^{n+1} to repeat steps (5) through (8). Check the solution convergence of ω^{n+1} and θ^{n+1} and if not converged, repeat steps (5)–(8).
10. Repeat steps (4)–(9) for advancing time levels until steady-state convergence is achieved.

To test and assess grid independence of the solution scheme, many numerical experiments were performed. These experiments showed that an equally spaced grid mesh of 81×81 is adequate to describe the flow and heat transfer processes correctly. Further increase in the number of grid points produced essentially the same results. Fig. 2 shows the grid dependence of the predictions for $Re = 400$ and $Da = 0.1$. It can be seen from this figure that by using lower than 81×81 grids the solutions for the velocity and temperature profiles are dependent on the mesh size. However, for mesh sizes greater than or equal to 81×81 the same results are produced. The convergence criterion employed to reach the steady-state solution was the standard relative error which is based on the maximum norm given by

$$\Delta = \frac{\|\Omega^{n+1} - \Omega^n\|_\infty}{\|\Omega^{n+1}\|_\infty} + \frac{\|\theta^{n+1} - \theta^n\|_\infty}{\|\theta^{n+1}\|_\infty} \leqslant 10^{-6} \tag{20}$$

where the operator $\|\eta\|_\infty$ indicates the maximum absolute value of the variable over all the grid points in the computational domain.

5. Validation tests

In order to verify the accuracy of the present numerical study, the present numerical procedure was validated by performing simulations for isothermal flow in a vertical square cavity with a driving lid for Reynolds number $Re = 1000$ and Grashof number $Gr = 100$. The results were compared with the finite-difference solution of Iwatsu et al. [15] in the absence of the porous medium and heat generation for Prandtl number $Pr = 0.71$ as shown in Fig. 3. This comparison reveals good agreement between the two numerical solutions. Moreover, Tables 1 and 2 clearly show a good agreement of the average Nusselt number measured at the top surface wall and the maximum values of the horizontal and vertical velocity components along the mid-sections of the cavity between the present solution and that of Iwatsu et al. [15]. Furthermore, Fig. 4 shows that the profiles of the horizontal velocity, temperature, and the vertical velocity at the mid-sections of the cavity of the present solution compare well with those reported by Iwatsu et al. [15]. As an additional check on the accuracy of the results, the convergence of the numerical solution is checked by performing an overall heat transfer balance inside the cavity. All of these favorable comparisons lend confidence in the accuracy of the numerical results of the present work.

6. Results and discussion

In this section, the numerical results for mixed convection heat transfer of a heat-generating fluid in a lid-driven cavity filled with a uniform porous medium are discussed. The non-dimensional controlling parameters for this investigation are the ratio Gr/Re^2 (sometimes called the Richardson number Ri), the Darcy number Da, and the internal Rayleigh number Ra_I. Figs. 5–8 show typical contour maps of the temperature and streamlines obtained numerically for various values of the Richardson and Darcy numbers. The effects of the Darcy number and the Richardson number are illustrated in these figures. In the absence of the porous medium and the internal heat generation, indicated by setting $Da = \infty$, and $Ra_I = 0$, the value of the Richardson number provides a measure of the importance of buoyancy-driven natural convection relative to the lid-driven forced convection. For very small values of Ri, Figs. 5–7 indicate that the buoyancy effect is overwhelmed by the mechanical effect of the sliding lid and the flow features are similar to those of a driven cavity viscous flow of a non-stratified fluid. The fluid flow in a two-dimensional lid-driven cavity is characterized by a primary recirculating eddy of the size of the cavity generated by the lid and minor eddies near the bottom corners. The isotherms are clustered near the bottom surface of the enclosure (see Fig. 7), which indicates steep temperature gradients in the vertical direction in this region. In the remaining area of the cavity, the temperature gradients are weak and this implies that the temperature differences are very small in the interior region of the cavity due to the vigorous effects

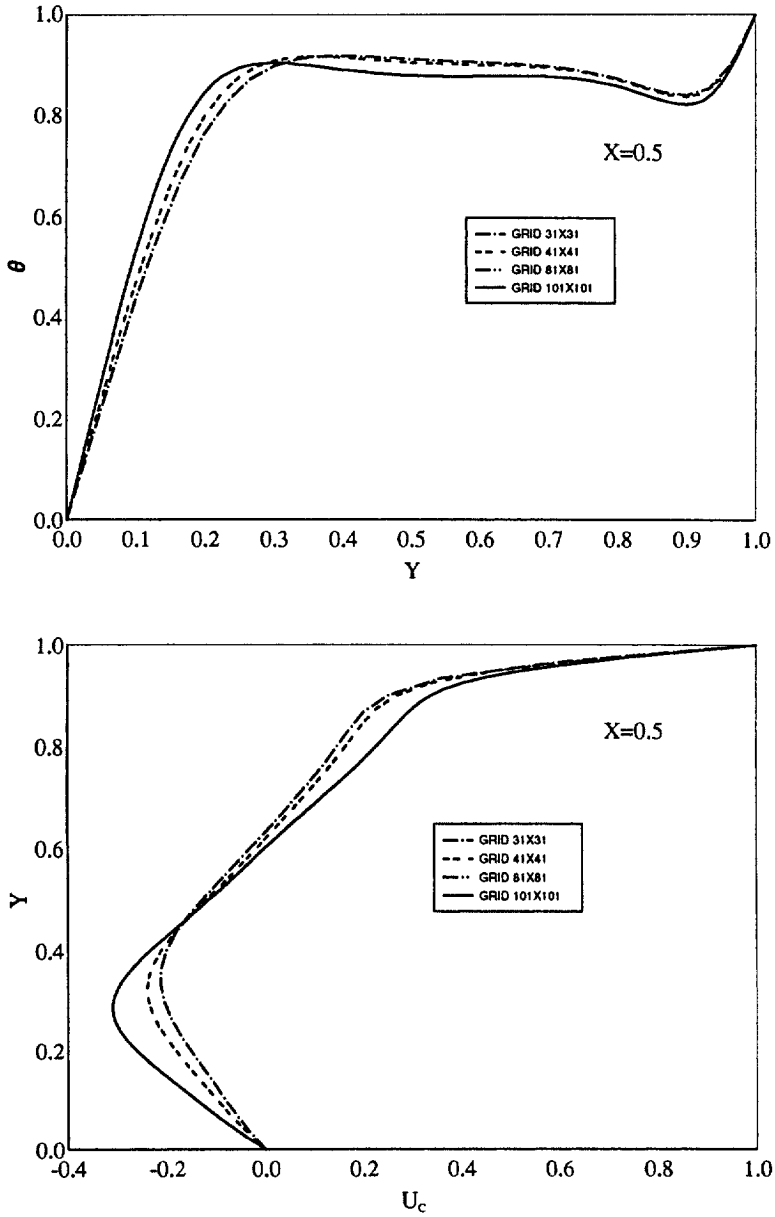

Fig. 2. Velocity and temperature profiles for various mesh sizes at $Re=400$ and $Da=0.1$.

of the mechanically-driven circulations. For large values of Ri (see Fig. 8), the buoyancy effect is dominant and the streamlines are almost stagnant in the bulk of the cavity interior except at portions close to the sliding top wall.

It is interesting to note that, as the Darcy number decreases, the flow circulation is progressively inhibited except at the portion close to the top surface by the flow retarding effect of the porous medium. For very small values of the Darcy number, the permeability of the medium approaches zero causing the flow eventually to cease in the bulk of the cavity. Also, Figs. 5–7 indicate that as $Da\rightarrow 0$, the convection heat transfer mechanism is almost suppressed and the isotherms are nearly parallel to the horizontal walls indicating that a quasi-conduction regime is reached. Moreover, the vertical temperature stratification is substantially linear in the stagnant bulk of the interior regions. This shows that the overall heat

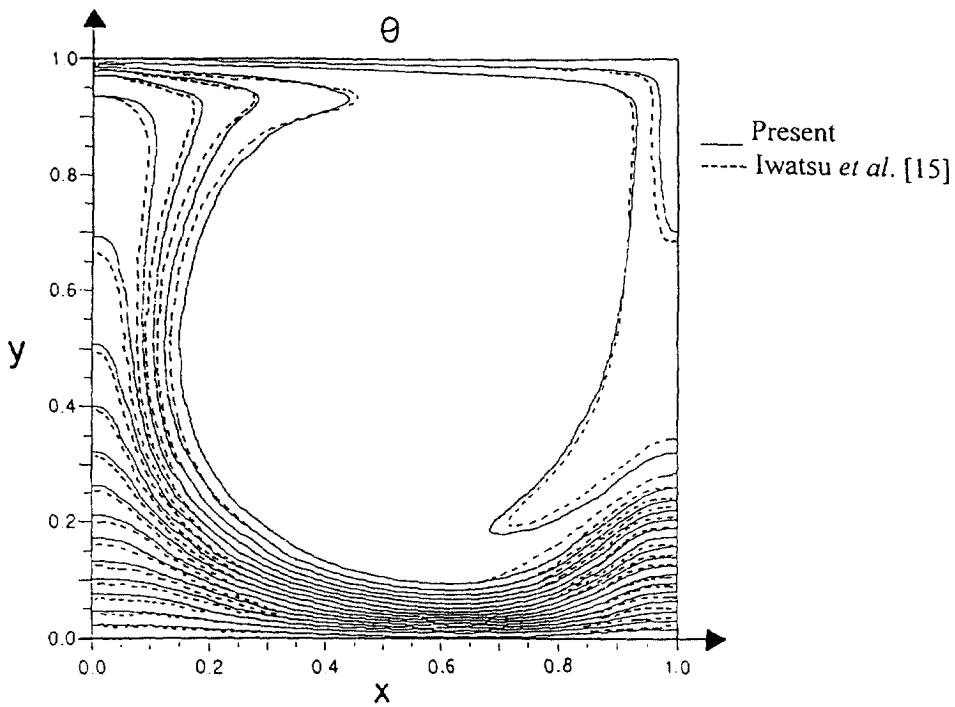

Fig. 3. Comparison of the isotherms between the present prediction and Iwatsu et al. [15] in the absence of porous medium and internal heat generation for $Re = 10^3$ and $Gr = 10^2$.

Table 1
Comparison of the average Nusselt number at the top surface between the present solution and that of Iwatsu et al. [15] for a vertical cavity at $Gr = 100$

Parameter	Present ($\overline{Nu}$)	Iwatsu et al. [15] ($\overline{Nu}$)
$Re = 100$	2.01	1.94
$Re = 400$	3.91	3.84
$Re = 1000$	6.33	6.33

is transferred by conduction in the middle and bottom parts of the cavity except in a relatively small region close to the top surface where the induced convective activities are appreciable. This means that the top plate velocity is adjusted in the same proportion to the convective velocity due to the internal heat generation.

The effect of internal heat generation on the flow patterns and isotherms for a Darcy number $Da = 0.1$, Grashof number $Gr = 100$, and a Reynolds number $Re = 1000$ is shown in Fig. 9. If the magnitude of the

Table 2
Comparison of the maximum and minimum values of the horizontal and vertical velocities at the mid-sections of the cavity between the present solution and those of Iwatsu et al. [15] for a vertical cavity at $Gr = 100$ and Reynolds number of 100 and 400, respectively

	$Re = 100$		$Re = 400$	
	Present	Iwatsu et al. [15]	Present	Iwatsu et al. [15]
U_{min}	−0.2122	−0.2037	−0.3099	−0.3197
U_{max}	1.000	1.000	1.000	1.000
V_{min}	−0.2506	−0.2448	−0.4363	−0.4459
V_{max}	0.1765	0.1699	0.2866	0.2955

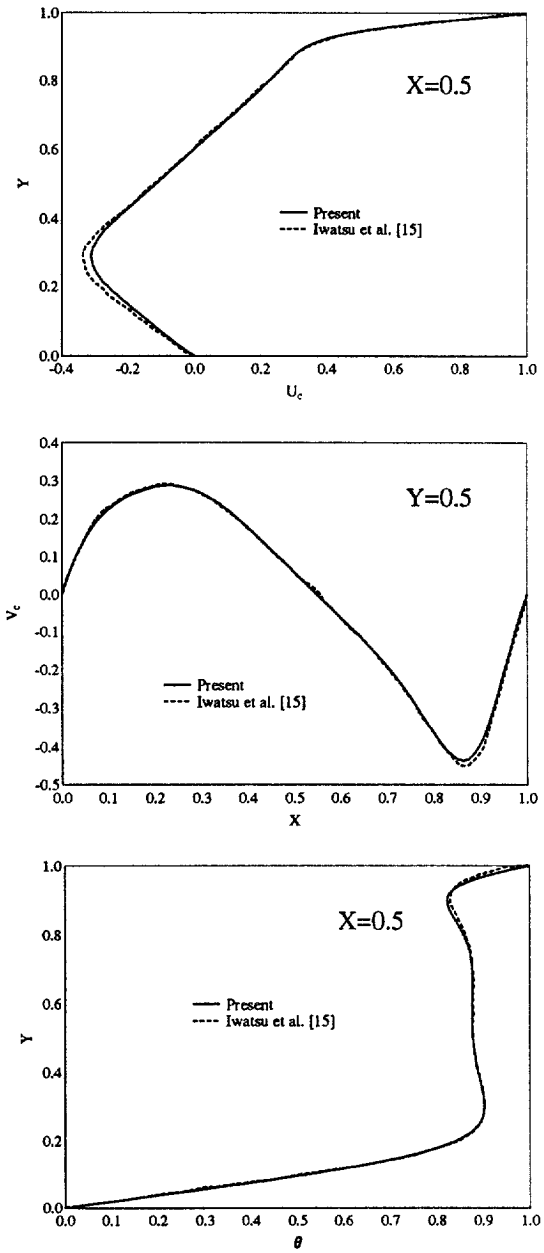

Fig. 4. Comparison of the present temperature and velocity profiles with Iwatsu et al. [15] in the absence of porous medium and internal heat generation for $Re=400$ and $Gr=10^2$.

internal Rayleigh number Ra_i is increased, the boundary layer is well established along the top and the bottom walls of the enclosure indicating sharp drops in the temperature near the horizontal walls. In addition, the isotherm plot indicates a localized region of high temperature (relative to the hot wall temperature) between the hot and cold surfaces. It can be seen from this figure that the streamlines remain unchanged since they are controlled by the value of the Richardson number Ri which is very small. This means that the top plate velocity is adjusted in the same proportion to the convective velocity due to the internal heat generation.

The effect of the Darcy number on the temperature and velocity profiles in a vertical cavity for various values of the Richardson number Ri at mid-sections of the cavity is depicted in Figs. 10–12. The presence of a porous medium within the cavity results in a force opposite to the flow direction which tends to resist the flow. This causes suppression in the thermal currents of the flow. This is clearly noticed from the horizontal and vertical velocity profiles at the center of the cavity as depicted in Fig. 10. Also, it is observed from Fig. 12 that as the Richardson number $Ri\to\infty$, the interior fluid is at rest and the corresponding temperature variation is linear indicating a conduction regime. On the other hand, when the buoyancy effect is minor, i.e. $Ri\ll 1$, most of the temperature variations are concentrated in narrow strips adjacent to the top and bottom lids. In the middle regions of the enclosure, the temperature variations are very small. These regions of almost uniform temperatures correspond to the portions in which the mechanically-induced activities are appreciable.

Finally, the effects of the inverse Darcy number $(1/Da)$ and the Richardson number Ri on the average Nusselt number are shown in Fig. 13. As discussed earlier, for a small Darcy number the only resistance to the flow is due to the porous medium and the resulting convective heat transfer is diminished which indicates a pure conduction regime. Furthermore, it is observed from Fig. 13 that for a fixed value of the Darcy number, the average Nusselt number increases with decreasing values of the Richardson number. This implies that the substantial contribution of convective heat transfer in the middle and upper portions of the cavity is manifest.

7. A heat transfer correlation

The numerically calculated heat transfer results were correlated for mixed convection in a vertical cavity and in the presence of the porous medium. It can be shown that the average Nusselt number is correlated as a function of both the inverse Darcy number $(Da^{-1}=1/Da)$ and the Richardson number $(Ri=Gr/Re^2)$ according to the following equation:

$$\overline{Nu}=\frac{1.6064}{(1+Da^{-1})^{0.1659}}(R_i)^{-0.1593}$$

for $10^{-4}\leqslant Da\leqslant 10^{-1}$. (21)

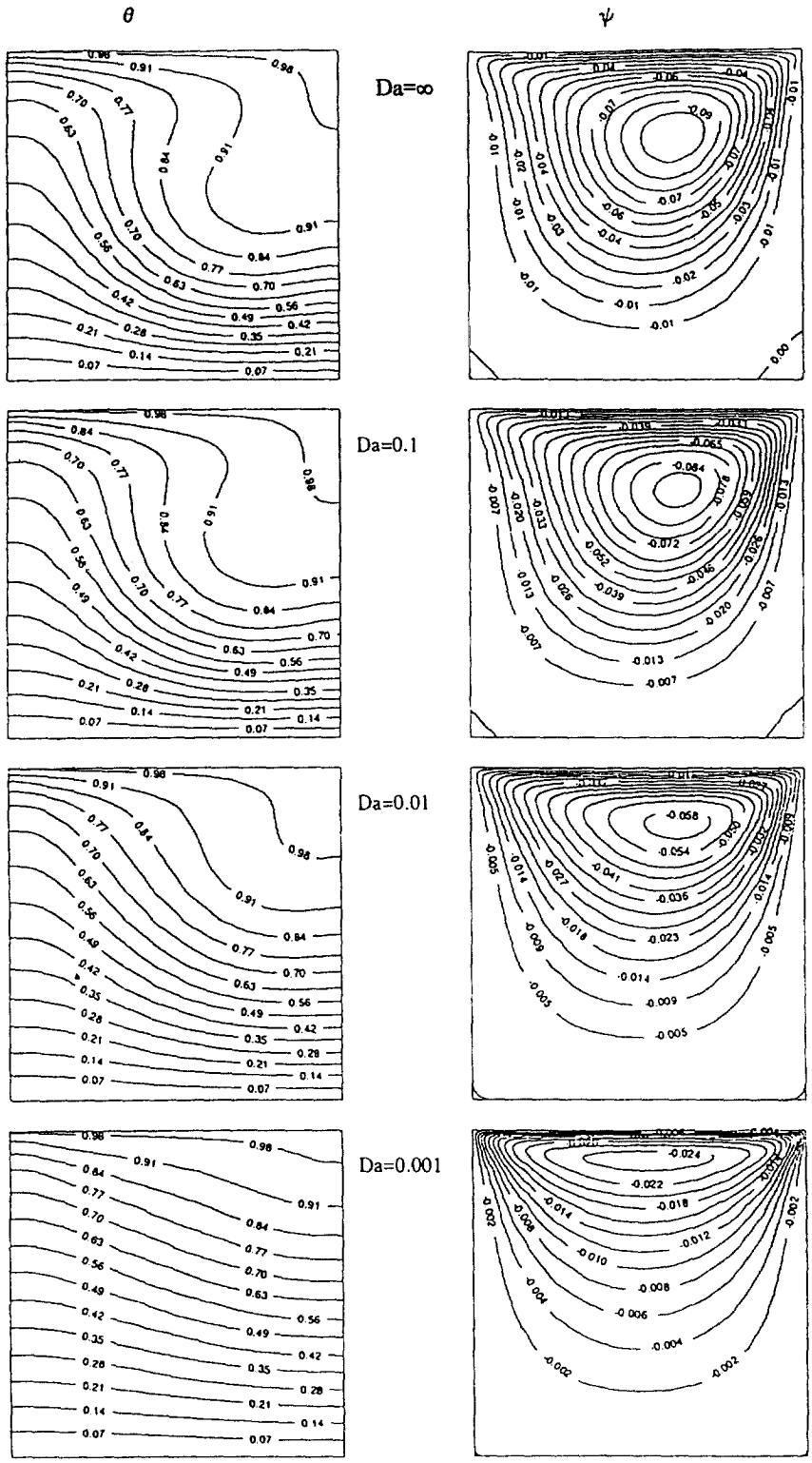

Fig. 5. Steady-state flow patterns and isotherms for various Darcy numbers at $Ri = 10^{-2}$ and $Ra_i = 0$.

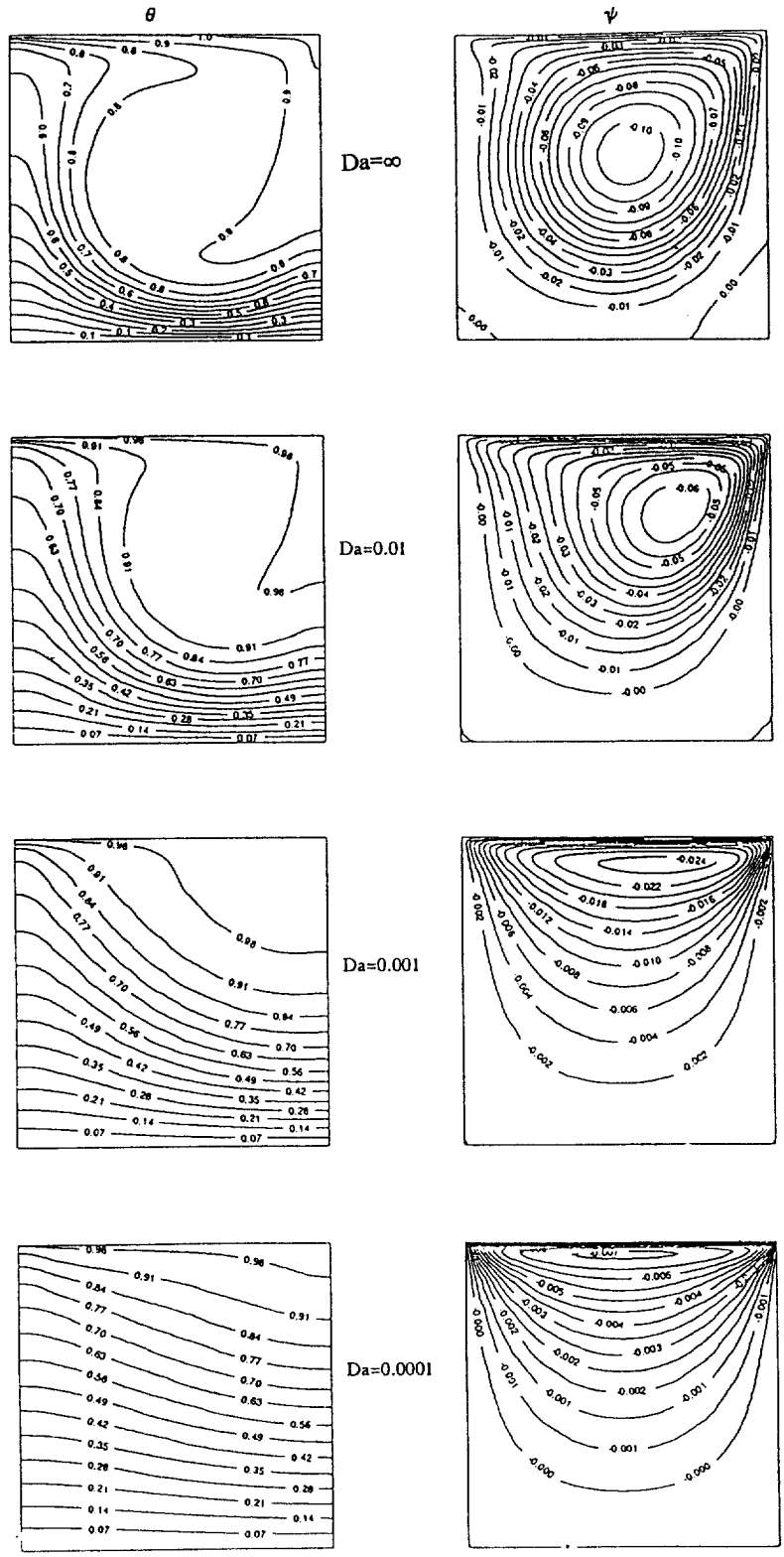

Fig. 6. Steady-state flow patterns and isotherms for various Darcy numbers at $Ri = 6.25 \times 10^{-4}$ and $Ra_1 = 0$.

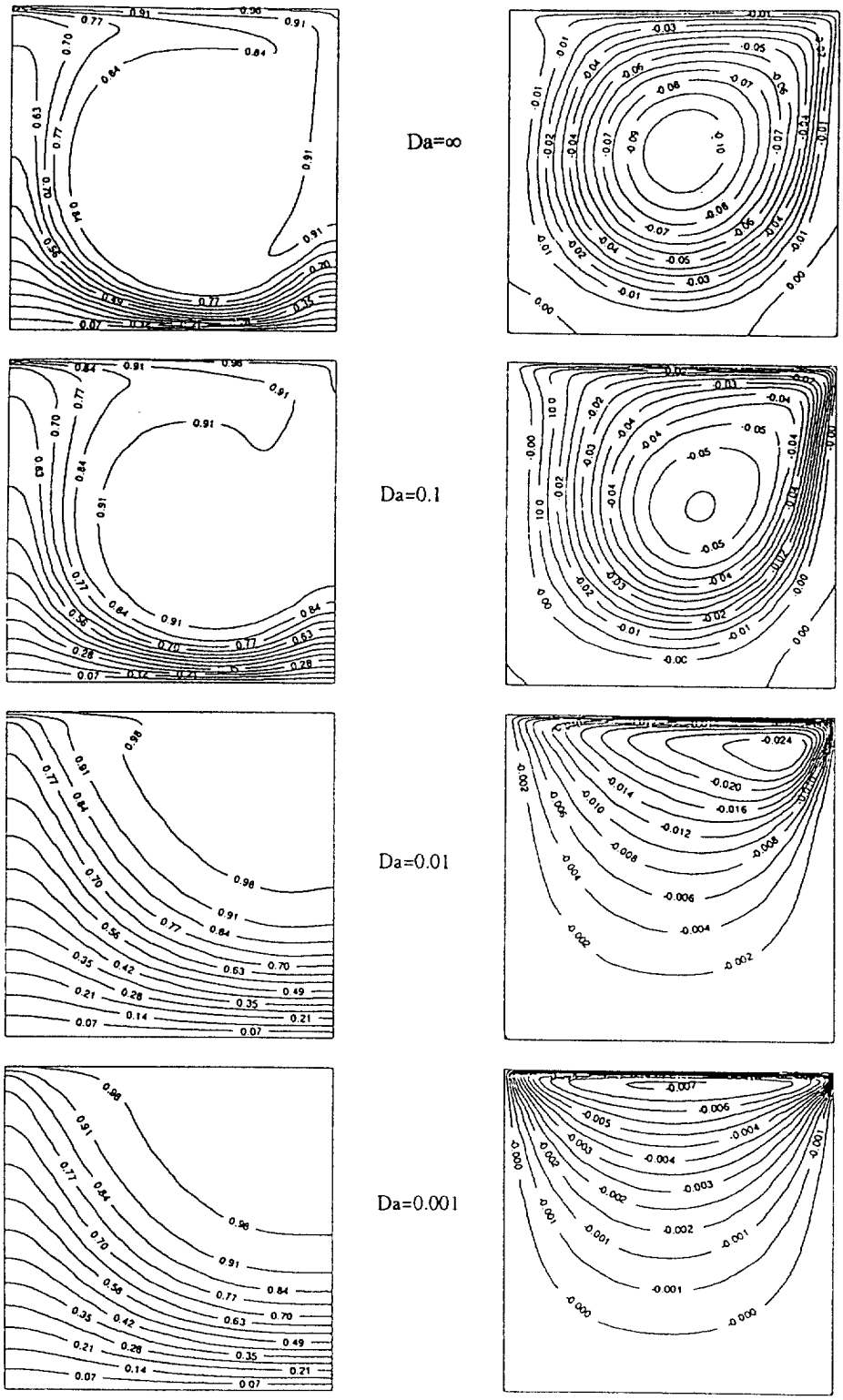

Fig. 7. Steady-state flow patterns and isotherms for various Darcy numbers at $Ri = 10^{-4}$ and $Ra_1 = 0$.

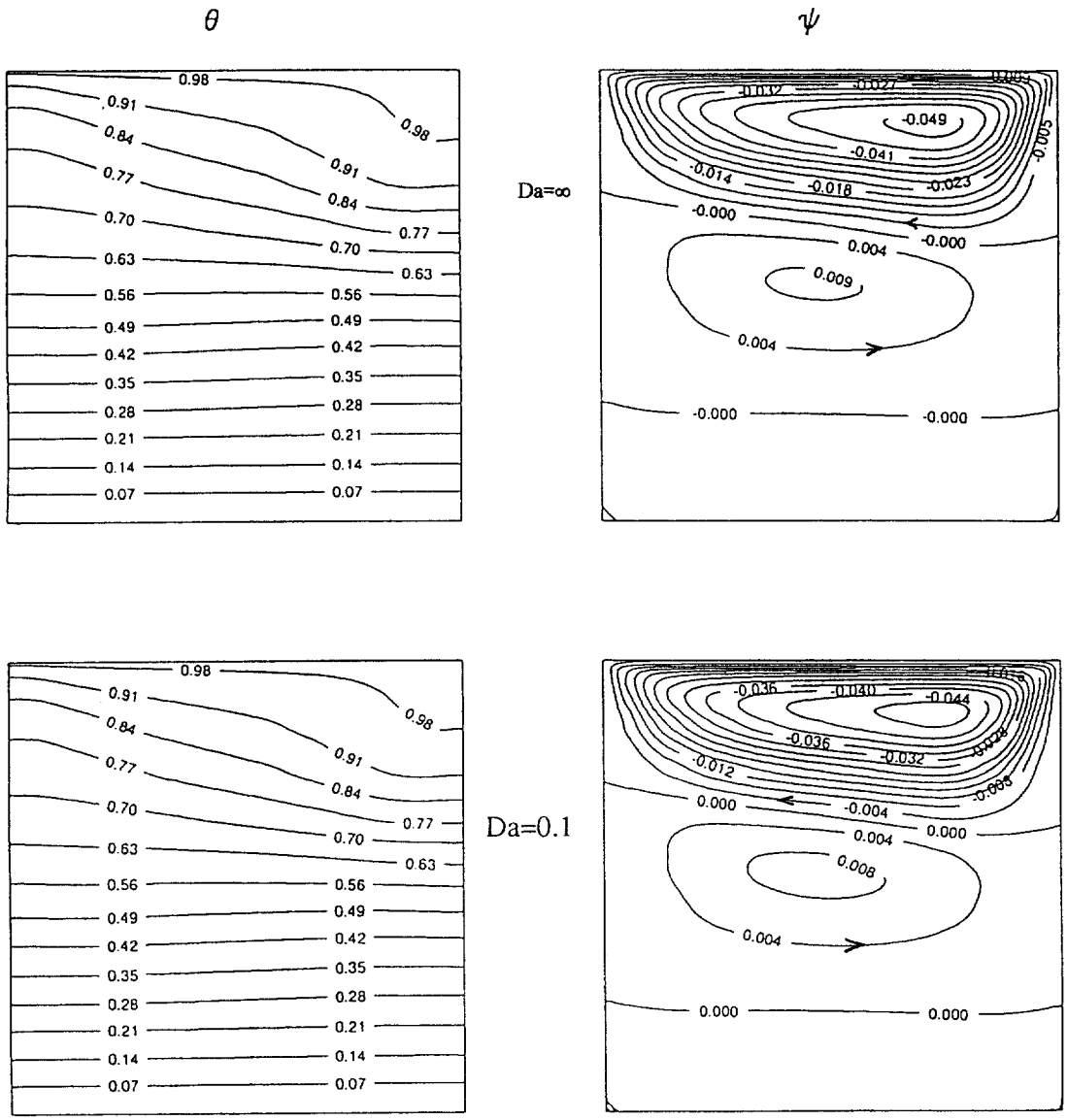

Fig. 8. Steady-state flow patterns and isotherms for various Darcy numbers at $Ri = 10$ and $Ra_t = 0$.

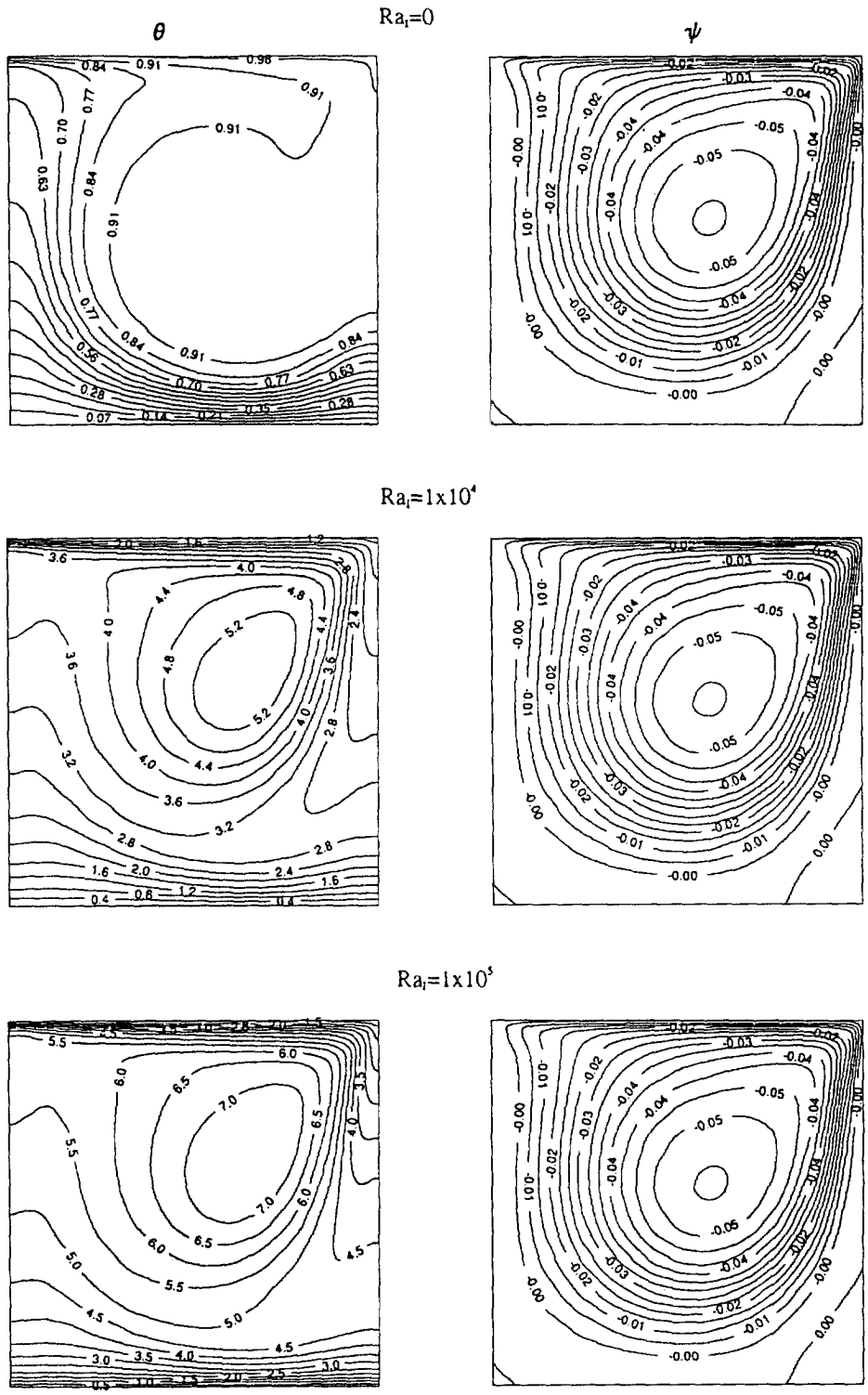

Fig. 9. Steady-state flow patterns and isotherms for various internal Rayleigh numbers at $Da=0.1$ and $Ri=10^{-4}$.

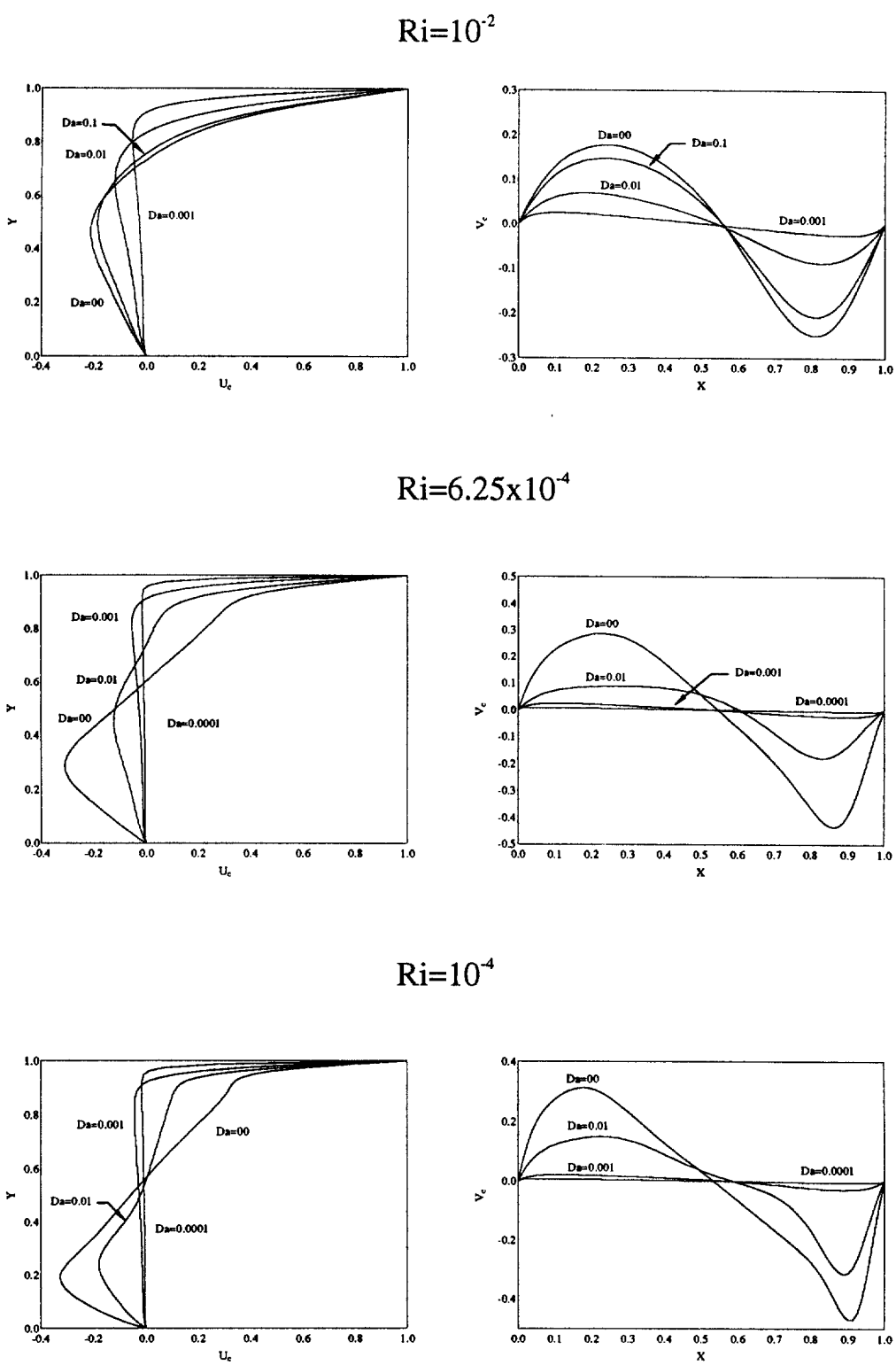

Fig. 10. Velocity profiles at mid-sections of the cavity for various *Da* and *Ri* at $Ra_1 = 0$.

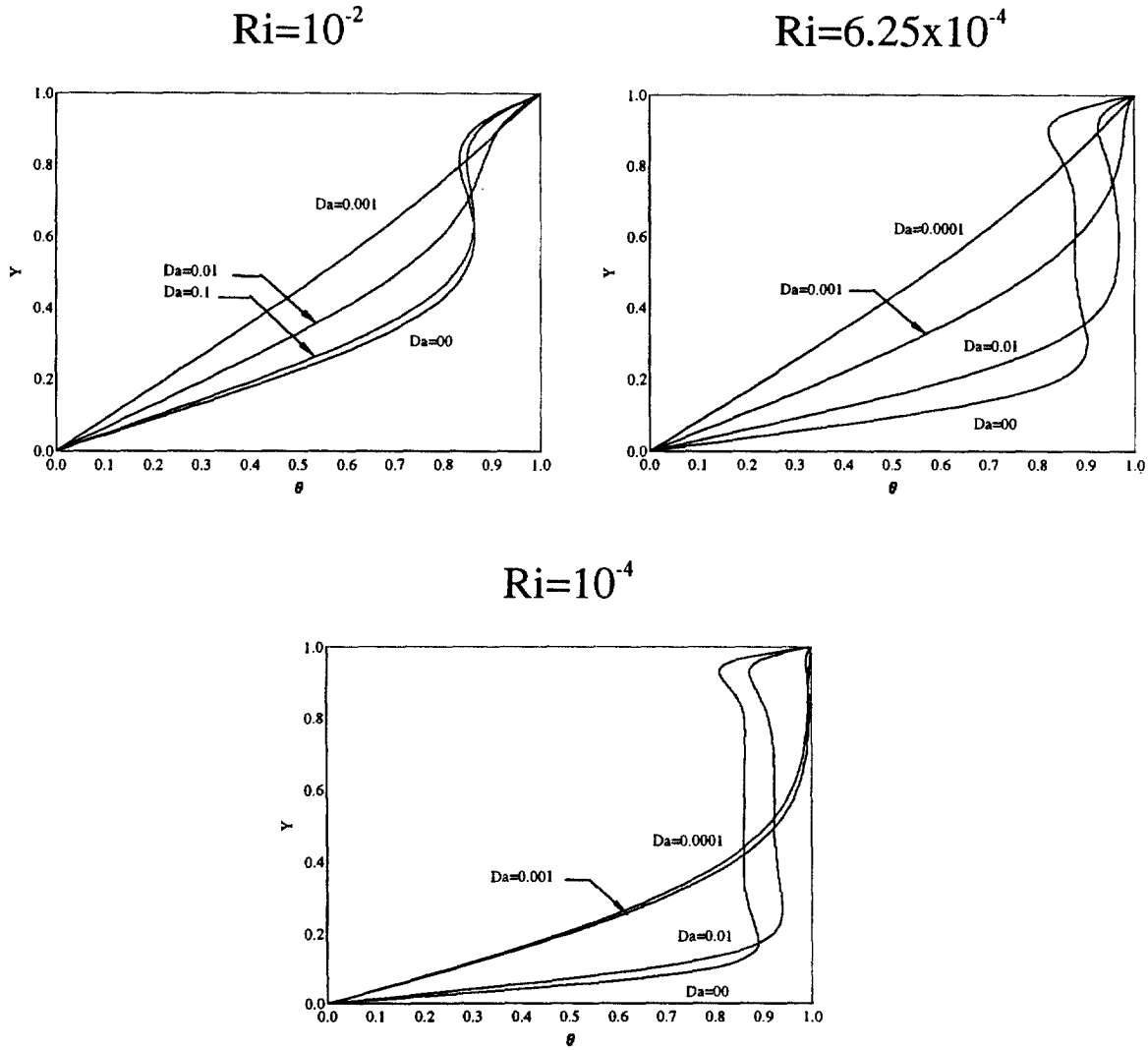

Fig. 11. Temperature profiles at mid-sections of the cavity for various Da and Ri at $Ra_1=0$.

8. Conclusions

The problem of unsteady mixed convective flow and heat transfer of a heat-generating fluid in a driven-lid cavity filled with a fluid-saturated porous medium was formulated and solved numerically. The finite-volume approach was employed along with the alternating direction implicit (ADI) scheme for the present problem. Comparisons with previously published work on special cases of the problem were performed and found to be in good agreement. Graphical results for various parametric conditions were presented and discussed. It was found that the heat transfer mechanisms and the flow characteristics inside the cavity are strongly dependent on the Richardson number. Also, significant suppression of the convective currents was obtained by the presence of a porous medium. Moreover, the presence of the internal heat generation in the model was found to have significant influence on the features of the isotherms and slight effects on the streamlines for small values of the Richardson number.

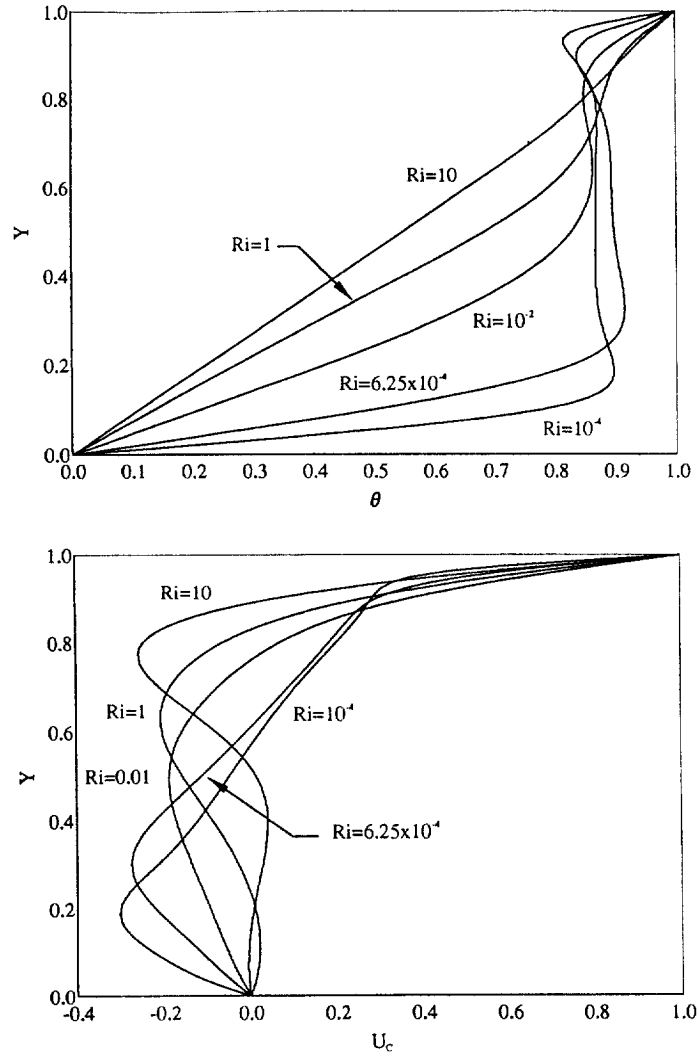

Fig. 12. Effect of Ri on the temperature and velocity profiles at mid-sections of the cavity for $Da=0.1$ and $Ra_1=0$.

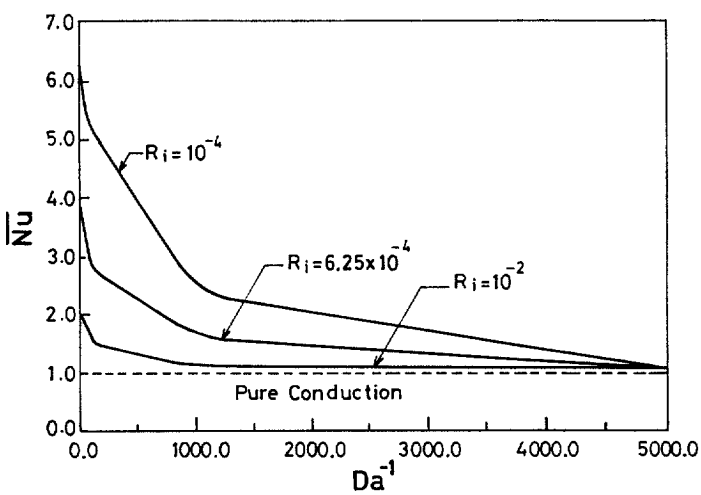

Fig. 13. Effect of *Ri* on the average Nusselt number for various Darcy numbers at $Ra_1=0$.

References

[1] C.K. Cha, Y. Jaluria, Recirculating mixed convection flow for energy extraction, Int. J. Heat Mass Transfer 27 (1984) 1801–1810.

[2] J. Imberger, P.F. Hamblin, Dynamics of lakes, reservoirs, and cooling ponds, A Rev. Fluid Mech. 14 (1982) 153–187.

[3] F.J.K. Ideriah, Prediction of turbulent cavity flow driven by buoyancy and shear, J. Mech. Engng Sci. 22 (1980) 287–295.

[4] L.A.B. Pilkington, Review Lecture: the float glass process, Proc. R. Soc. Lond. IA 314 (1969) 1–25.

[5] R.K. Agarwal, A third-order-accurate upwind scheme for Navier–Stokes solutions at high Reynolds numbers, AIAA-81-0112, in: Proc. 19th AIAA Aerospace Sciences Meeting, St Louis, MI, January, 1981.

[6] D.L. Young, J.A. Liggett, R.H. Gallagher, Unsteady stratified circulation in a cavity, ASCE J. The Engineering Mechanics Division 102 (EM6) (1976) 1009–1023.

[7] M. Morzynski, CzO Popiel, Laminar heat transfer in a two-dimensional cavity covered by a moving wall, Numer. Heat Transfer 13 (1988) 265–273.

[8] M.C. Thompson, J.H. Ferziger, An adaptive multigrid technique for the incompressible Navier–Stokes equations, J. Comput. Phys. 82 (1989) 94–121.

[9] U. Ghia, K.N. Ghia, C.T. Shin, High-*Re* solutions for incompressible flow using Navier–Stokes equations and a multigrid method, J. Comput. Phys. 43 (1982) 387–411.

[10] R. Schreiber, H.B. Keller, Driven cavity flows by efficient numerical techniques, J. Comput. Phys. 49 (1983) 310–333.

[11] J.R. Kosef, R.L. Street, The lid-driven cavity flow: a synthesis of qualitative and quantitative observations, ASME J. Fluids Engng 106 (1984) 390–398.

[12] K. Torrance, R. Davis, K. Elike, P. Gill, D. Gutman, A. Hsui, S. Lyons, H. Zien, Cavity flows driven by buoyancy and shear, J. Fluid Mech. 51 (1972) 221–231.

[13] A.K. Prasad, J.R. Koseff, Combined forced and natural convection heat transfer in a deep lid-driven cavity flow, in: Heat Transfer in Convective Flows, HTD-107, ASME, New York, 1989, pp. 155–162.

[14] M.K. Moallemi, K.S. Jang, Prandtl number effects on laminar mixed convection heat transfer in a lid-driven cavity, Int. J. Heat Mass Transfer 35 (1992) 1881–1892.

[15] R. Iwatsu, J.M. Hyun, K. Kuwahara, Mixed convection in a driven cavity with a stable vertical temperature gradient, Int. J. Heat Mass Transfer 36 (1993) 1601–1608.

[16] S. Kakac, W. Aung, R. Viskanta, in: Natural Convection: Fundamentals and Applications, Hemisphere, Washington, DC, 1985, pp. 475–611.

[17] A. Bejan, Convective Heat Transfer, in: 1st ed., Chap. 11, Wiley, New York, 1984.

[18] P. Cheng, Heat Transfer in Geothermal Systems, Advances in Heat Transfer 4 (1978) 1–105.

[19] D.A. Nield, A. Bejan, Convection in Porous Media, in: Springer, New York, 1992.

[20] K. Vafai, C.L. Tien, Boundary and inertia effects on flow and heat transfer in porous media, Int. J. Heat Mass Transfer 24 (1981) 195–203.

[21] T.K. Aldoss, M.A. Al-Nimr, M.A. Jarrah, B.J. Al-Shaer, Magnetohydrodynamic mixed convection from a plate embedded in a porous medium, Numerical Heat Transfer 28 (1995) 635–645.

[22] W.J. Minkowycz, P. Cheng, C.H. Cheng, Mixed convection about a nonisothermal cylinder and sphere in a porous medium, Numerical Heat Transfer 8 (1985) 349–359.

[23] F.C. Lai, F.A. Kulacki, Non-Darcy mixed convection along a vertical wall in a saturated porous medium, Int. J. Heat Mass Transfer 113 (1991) 252–255.

[24] J.C. Hsieh, T.S. Chen, B.F. Armaly, Nonsimilarity solutions for mixed convection from vertical surface in a porous medium–variable surface temperature of heat flux, Int. J. Heat Mass Transfer 36 (1993) 1485–1493.

[25] A.J. Chamkha, Non-Darcy hydromagnetic free convection from a cone and a wedge in porous medium, Int. Commun. Heat Mass Transfer 23 (1996) 875–887.

[26] J.L. Lage, Effect of the convective inertia term on Benard convection in a porous medium, Numerical Heat Transfer 22 (1992) 469–485.

[27] B.K.C. Chan, C.M. Ivey, J.M. Barry, Natural convection in enclosed porous media with rectangular boundaries, ASME J. Heat Transfer 2 (1970) 21.

[28] S.V. Patankar, Numerical Heat Transfer and Fluid Flow, Hemisphere, Washington, DC, 1980.